Transactions of NAMP 24, (2026) 101-118

Transactions of
The Nigerian Association of
Mathematical Physics
Journal homepage: https://nampjournals.org.ng

EFFECTS OF VARIABLE VISCOSITY AND THERMAL CONDUCTIVITY ON MOTION OF CASSON NANOFLUID THROUGH A RIGA SURFACE WITH HEAT FLUX THEORY

Michael Adesola Taiwo[1], Toyin Wasiu Akaje[2*], Bakai Ishola Olajuwon[3], Musiliu Tayo Raji[4], Olamilekan Fagbemiro[5]

[1,2,3,4,5]*Federal University of Agriculture, Abeokuta, Ogun State, Nigeria.*

ARTICLE INFO

Article history:
Received xxxxx
Revised xxxxx
Accepted xxxxx
Available online xxxxx

Keywords:
Casson nanofluid,
Riga surface,
Variable viscosity,
Variable thermal conductivity.
Cattaneo–Christov heat flux,
Spectral collocation method.

ABSTRACT

This study examines the influence of variable viscosity and thermal conductivity on the flow and heat transfer characteristics of Casson nanofluid over a Riga surface embedded in a porous medium, incorporating the Cattaneo–Christov heat flux model. The governing partial differential equations, formulated under the Boussinesq and boundary layer approximations with consideration of nonlinear buoyancy, first-order chemical reaction, thermophoresis, and Soret–Dufour effects, are transformed into a system of ordinary differential equations using similarity transformations. These equations are solved numerically via the Chebyshev spectral collocation method. Parametric investigations reveal that increasing the modified Hartmann number enhances the velocity profile and hydrodynamic boundary layer thickness, while higher Casson parameters elevate skin friction but resist fluid motion under constant viscosity and thermal conductivity. Elevated Prandtl and Schmidt numbers suppress both velocity and temperature fields, whereas greater thermal radiation, Eckert number, and thermal relaxation time enhance thermal boundary layer growth. Variable viscosity is found to intensify fluid motion, and variable thermal conductivity amplifies both temperature and velocity distributions. Results also highlight the opposing roles of chemical reaction and thermophoresis parameters on concentration and velocity fields. Comparison with previous studies confirm the accuracy of the present model. The findings provide valuable insight into the behaviour of non-Newtonian nanofluids under complex thermal and magnetic conditions, with potential applications in energy systems, biomedical flows, and advanced material processing.

1. INTRODUCTION

The study of non-Newtonian fluids has attracted significant attention in recent years due to their complex rheological behaviour and broad industrial applications. Unlike Newtonian fluids, their viscosity is not constant but depends on the applied shear rate. Examples include paints, ketchup, blood, and polymeric suspensions. Among these, the **Casson fluid model** is widely used to describe the flow of yield-stress materials encountered in food processing, biomedical systems, and coating technologies.

*Corresponding author: TOYIN WASIU AKAJE
E-mail address: akajewasiu@gmail.com
https://doi.org/10.60787/tnamp.v24.671

Because of its nonlinearity, most analyses of such fluids rely on numerical or semi-analytical methods to explore their transport phenomena under various boundary conditions. Several researchers have examined Casson and related non-Newtonian fluid flows under different physical effects. For instance, Raju *et al.* [1] examined" heterogeneous-homogeneous reactions on the stagnation motion of Casson fluid. Mahanta and Shaw [2] presented research on 3D Casson fluid motion through a porous linearly stretchable sheet with convective boundary condition. Bhatti *et al.* [3] addressed" peristaltic blood flow with the Casson model with entropy generation and magnetohydrodynamic significance. Chemically reactive species diffusion on Casson fluid flow past an unsteady stretching surface in a passable medium "has been addressed by Makanda *et al.* [4]. Rashidi *et al* [5] studied stretchable sheets by examining the significance of the Soret-Dufour mechanism. The simultaneous flow of Casson-Walters-B non-Newtonian fluids under the influence of Soret-Dufour mechanisms was examined by Idowu and Falodun [6] when the viscosity and thermal conductivity varied. Falodun *et al.* [7] studied MHD Casson fluid flow past a half-infinite vertical plate numerically.

The significance of MHD is the migration of a conductor into a magnetic field, while an electric current can induce a magnetic field. When current is induced due to the electrically conducting fluid motion subject to the magnetic field, it produces the Lorentz force. The Lorentz force acts like a resistive force, which slows down the motion of the fluid. A fixed magnet together with an alternate electrode on a surface is called a Riga surface. Fixed magnets play a significant role in industrial and technological applications. MHD finds important applications in crystal growth, power generators, electromagnetic pumps and so on. Due to these applications, many researchers have concentrated their work on the significance of MHD on non-Newtonian fluids in recent times. The significance of the MHD radiative motion of a hybrid nanofluid over a rotating disk was addressed by Waqas *et al.* [8]. A parametric study of hybrid nanofluid flow with a magnetic field past a fluctuating spinning disk was conducted by Zhang *et al.* [9]. Ramzan *et al.* [10] elucidated the heat transfer phenomenon of a mixed convective flow of MHD hybrid nanofluid over a stretching sheet. Jamshed *et al.* [11] have investigated the Cattaneo-Christov heat flux significance on engine oil-based Williamson hybrid nanofluids. Kumar *et al.* [12] researched the hydromagnetic unsteady slip stagnation flow of nanofluid. Ali and Sandeep [13] studied the Cattaneo-Christov model for radiative heat transfer of MHD Casson-ferrofluid.

Loganathan and Deepa [14] studied Casson fluid flow past a Riga plate with variable chemical reactions. Eswaramoorthi *et al.* [15] conducted analytical and numerical analysis for the Darcy-Forchheimer flow of Williamson fluid over a Riga plate with Cattaneo-Christov theories. Heat generation, thermal radiation, and the variable thermal conductivity characteristic are amplified, which reduces the temperature field. Studied 3D heat transfer analysis of viscoelastic nanofluid flows past a convectively heated Riga porous plate with Cattaneo-Christov double flux. The study of Rasool and Zhang [16] examined the characteristics of a chemical reaction and convective boundary conditions in Powell-Eyring nanofluid flow along a radiative Riga plate.

Although much research has been done on Casson nanofluids, few studies have examined the combined effects of variable viscosity and thermal conductivity with nonlinear buoyancy, Cattaneo–Christov flux, and Soret–Dufour mechanisms over a Riga plate. These interconnected effects are crucial in modern energy systems and biomedical engineering, where temperature-dependent viscosity and conductivity significantly impact heat and mass transfer rates.

Hence, the novelty of the present research lies in:

i. Formulating a comprehensive Casson nanofluid model over a Riga plate embedded in a porous medium, incorporating variable viscosity and thermal conductivity;
ii. Integrating nonlinear buoyancy effects along with Soret–Dufour mechanisms to capture complex double-diffusive phenomena;
iii. Applying the Cattaneo–Christov heat flux model to achieve a more realistic description of thermal relaxation behaviour, and
iv. Employing the Chebyshev spectral collocation method for accurate numerical resolution of the governing nonlinear equations.

This unique combination of variable thermo-physical properties, nonlinear buoyancy, Cattaneo–Christov heat flux, and Riga surface magnetodynamics for a Casson nanofluid has not been comprehensively reported in previous literature. The present work thus bridges this gap by analysing the synergistic effects of these parameters on velocity, temperature, and concentration fields, offering new physical insights relevant to energy conversion, advanced material manufacturing, and biomedical flow systems.

1.1 Mathematical analysis

Falodun and Omowaye, [17]. The coordinate system of the problem is (x,y), where the x-coordinate is utilised along the Riga plate, while the y-coordinate is normal to it. The physics of the problem in a vertical stretching Riga surface is illustrated in Figure 1. T_w and C_w are denoted to be the wall temperature and concentration, while C_∞ and T_∞ are the ambient concentration and temperature, respectively. A nonlinear buoyancy force is considered in this study with the presence of a first-order chemical reaction. A scenario whereby $T_w > T_\infty$ and $C_w > C_\infty$, which means a heated Riga surface, is considered in this study. The viscosity and thermal conductivity existing within the boundary layer are considered to vary. The Lorentz force is used in conjunction with the Grinberg term in this study. The Boussinesq and boundary layer approximation is valid. Based on viscosity $\left(\tau = \mu \frac{\partial u}{\partial y}|_y = 0\right)$, the rheological equation of a Casson liquid, as discussed in Idowu and Falodun (2020), is:

$$\tau_{ij} = \left(\mu_b(T) + \frac{P_y}{\sqrt{2\pi}}\right) 2e_{ij} \quad when \quad \pi > \pi_c$$

$$\tau_{ij} = \left(\mu_b(T) + \frac{P_y}{\sqrt{2\pi_c}}\right) 2e_{ij} \quad when \quad \pi < \pi_c \tag{1}$$

Here, P_y signifies the yield stress of the liquid, which is

$$P_y = \frac{\mu_b(T)\sqrt{(2\pi)}}{\gamma} \tag{2}$$

μ_b indicates plastic dynamic Casson viscosity, $\pi = e_{ij}e_{ij}$ indicates the multiplication of deformation rate, both together, and e_{ij} indicates the deforming rate, and π_c indicates the critical value of Casson liquid. The Casson liquid flow when $\pi > \pi_c$, we have

$$\mu_0 = \mu_b(T) + \frac{P_y}{\sqrt{2\pi}} \tag{3}$$

invoking eqn (2) in (3), the viscosity becomes subject to plastic dynamic Casson viscosity μ_b, the density ρ and the Casson term γ gives

$$\mu_0 = \frac{\mu_b(T)}{\rho}\left(1+\frac{1}{\gamma}\right) \tag{4}$$

The heat flux on the fluid motion is based on the utilisation of Rosseland approximation as explored in Akaje et al. [19] and Fagbade et al. [7], and:

$$q_r = -\frac{4\sigma_s}{3k_e}\frac{\partial T^4}{\partial y} \tag{5}$$

Where Stefan-Boltzmann constant=σ_s, mean absorption coefficient=k_e. It is summarised that the differences between temperatures in the fluid motion are small, and T^4 could be written in a linear function by simplifying T^4 about T_∞ by employing the Taylor series and foregoing terms of higher order to give

$$T^4 \cong 4T_\infty^3 T - 3T_\infty^4 \tag{6}$$

Substituting (6) into (5), the energy equation becomes

$$-\frac{\partial q_r}{\partial y} = \frac{16\sigma_s T_\infty^3}{3k_e}\frac{\partial^2 T}{\partial y^2} \tag{7}$$

Based on the exploration of Idowu and Falodun [6], V_T in the concentration equation is given as

$$V_T = -k\nu\frac{\nabla T}{T_{ref}} = -\frac{k\nu}{T_{ref}}\frac{\partial T}{\partial y} \tag{8}$$

where k denotes the thermophoretic coefficient given as

$$k = \frac{2C_s\left(\frac{\lambda_g}{\lambda_p}+C_tK_n\right)\left[1+K_n\left(C_1+C_2e^{\frac{-C_3}{K_n}}\right)\right]}{(1+3C_mK_n)\left(1+2\frac{\lambda_g}{\lambda_p}+2C_tK_n\right)} \tag{9}$$

$C_1,\ C2, C3, Cm, C_s,\ C_t$ are constants, λ_g and λ_p denote fluid thermal conductivities and diffused particles, and K_n denote the Knudsen number.

Based on all the assumptions above, the equations that govern the present model are:

$$\frac{\partial u}{\partial x}+\frac{\partial v}{\partial y} = 0 \tag{10}$$

$$\rho\left(u\frac{\partial u}{\partial x}+v\frac{\partial u}{\partial y}\right) = \left(1+\frac{1}{\beta}\right)\frac{\partial}{\partial y}\left(\mu\frac{\partial u}{\partial y}\right)+g\rho[\beta_1(T-T_\infty)+\beta_2(T-T_\infty)^2]+g\rho[\beta_3(C-C_\infty)+\beta_4(C-C_\infty)^2]+\frac{\pi J_0M_0}{8\rho_{nf}}\exp\left(-\frac{\pi}{r_0}y\right) \tag{11}$$

$$u\frac{\partial T}{\partial x}+v\frac{\partial T}{\partial y} = \frac{1}{\rho c_p}\frac{\partial}{\partial y}\left(K\frac{\partial T}{\partial y}\right)+\frac{Dk_T}{c_sc_p}\frac{\partial^2 C}{\partial y^2}+\frac{\mu}{\rho c_p}\left(1+\frac{1}{\beta}\right)\left(\frac{\partial u}{\partial y}\right)^2-\frac{1}{\rho c_p}\frac{\partial q_r}{\partial y}+\frac{Q}{\rho c_p}(T-T_\infty)-\beta_5\left[u\frac{\partial u}{\partial x}\frac{\partial T}{\partial x}+v\frac{\partial v}{\partial y}\frac{\partial T}{\partial y}+u\frac{\partial v}{\partial x}\frac{\partial T}{\partial x}+v^2\frac{\partial^2 T}{\partial y^2}+v\frac{\partial u}{\partial y}\frac{\partial T}{\partial x}+2uv\frac{\partial^2 T}{\partial y\partial x}+u^2\frac{\partial^2 T}{\partial x^2}\right]+\tau\left[D_B\left(\frac{\partial C}{\partial y}\right)\left(\frac{\partial T}{\partial y}\right)+\frac{D_T}{T_\infty}\left(\frac{\partial T}{\partial y}\right)^2\right] \tag{12}$$

$$u\frac{\partial C}{\partial x}+v\frac{\partial C}{\partial y} = D\frac{\partial^2 C}{\partial y^2}+\frac{D_T}{T_\infty}\frac{\partial^2 T}{\partial y^2}+\frac{Dk_T}{T_m}\frac{\partial^2 T}{\partial y^2}-K'(C-C_\infty)-\frac{\partial(V_TC)}{\partial y} \tag{13}$$

Subject to:

$$u = U_w(x) = Bx \quad , v = -v(x) \quad , T = T_w \quad , C = C_w \quad , aty = 0 \tag{14}$$

$$u \to 0 \quad , T \to T_\infty \quad , C \to C_\infty \quad , asy \to \infty \tag{15}$$

u and v represent the relations $u = \frac{\partial \psi}{\partial y}$ and $v = -\frac{\partial \psi}{\partial x}$. This definition of u and v, the free stream is $\psi(x, y)$. It automatically satisfies the continuity equation. The following variables are utilised in the model

$$\eta = \left(\frac{B}{\nu}\right)^{\frac{1}{2}} y \quad , \psi = (\nu B)^{\frac{1}{2}} x f(\eta), \ \theta(\eta) = (\mathrm{T} - T_\infty)(T_w - T_\infty)^{-1} \ , \phi(\eta) = (\mathrm{C} - C_\infty)(C_w - C_\infty)^{-1} \tag{16}$$

$$\mu(T) = \mu^*[a - b(T_\infty - T)], \ K(T) = K^*[1 - d(T_\infty - T)], \ D(T) = D^*[1 + c(T - T_\infty)] \tag{17}$$

The wall temperature (T_w), concentration (C_w), and ambient temperature T_∞ and concentration C_∞ as defined in Falodun and Omowaye [17] are given as:

$$T_w = T_0 + m_1 x, \ C_w = C_0 + m_3 x, \ T_\infty = T_0 + m_2 x, \ C_\infty = C_0 + m_4 x \tag{18}$$

Employing equations (16)-(18) above on the flow governing equations (10)-(13) subject to (14) and (15) to obtain:

$$\left(1 + \frac{1}{\beta}\right)(1 + \xi_1\theta) f''' + \alpha_1\theta^2 + \alpha_2\phi^2 - 2(f')^2 + \xi_1\left(1 + \frac{1}{\beta}\right) f''\theta' + Gr\theta + Gc\phi + M_q \exp(-\varepsilon\eta) = 0 \tag{19}$$

$$\left(\frac{(1+\xi_2\theta)+R}{Pr}\right)\theta'' + f\theta' + \frac{1}{Pr}\xi_2(\theta')^2 + Ec(1 + \xi_1\theta)\left(1 + \frac{1}{\beta}\right)(f''^2) + Nt(\theta')^2 + \mathrm{Pr}He\theta + Do\phi'' + \mathrm{Q}\theta - \gamma(ff'\theta' + ff\theta'') = 0 \tag{20}$$

$$\phi'' + Scf\phi' - ScCr\phi + \frac{ScNtSo}{LnNb}\theta'' + \tau[\phi\theta'' + \theta'\phi'] = 0 \tag{21}$$

subject to:

$$f' = 1 \quad , f = S_w \quad , \theta = 1 \quad , \phi = 1 \quad , at\eta = 0 \tag{22}$$

$$f' \to 0 \quad \theta \to 0 \quad , \phi \to 0 \quad , as\eta \to \infty \tag{23}$$

Note that: $\xi_1 = b(T_w - T_\infty) = \text{temperature} - \text{dependent variable viscosity}$, $So = \frac{Dk_T(T_w - T_\infty)}{T_w\nu(C_w - C_\infty)} = \text{Soret number}$, $Gr = \frac{2g\beta_1 L(T_w - T_\infty)}{U_w^2 e^{\frac{2x}{L}}} = \text{thermal Grashof number}$, , $Nt = \frac{D_T(T_w - T_\infty)}{T_\infty\nu} = \text{Brownian motion parameter}$, $Gc = \frac{2g\beta_2 L(C_w - C_\infty)}{U_w^2 e^{\frac{2x}{L}}} = \text{mass Grashof}$, $M_q = \frac{\pi J_0 M_0}{8\rho_j x a^2} = \text{modified Harmann number}$,

, $2 = dTw - T\infty = \text{temperature} - \text{dependent}$ varied thermal conductivity, $R = \frac{16\sigma_s T_\infty^3}{3k_e} = \text{thermal radiation term}$, , $Do = \frac{Dk_T(C_w - C_\infty)}{\nu c_s c_p(T_w - T_\infty)} = \text{Dufour}$, $Pr = \frac{\nu\rho c_p}{k^*} =$ Prandtl , $Sc = \frac{\nu}{D^*} = \text{Schmidt}$, $Ec = \frac{U_w^2}{c_p(T_w - T_\infty)} = \text{Eckert}$, $Ln = \frac{\nu}{D_B} = \text{Lewis number}$, $Nb = \frac{D_B(C_w - C_\infty)}{\nu} =$ thermophoretic term, $\alpha_1 = \frac{g\beta_3 \mathrm{L}(T_w - T_\infty)^2}{U_w^2 e^{\frac{2x}{L}}} =$

nonlinear convective parameter for temperature, $\alpha_2 = \frac{gL\beta_c(C_w - C_\infty)^2}{U_w^2 e^{\frac{2x}{L}}} =$

nonlinear convective parameter for concentration, $\gamma = \beta_5 B = heat$ thermal ralaxation. The engineering views are the skin friction, Sherwood, and Nusselt magnitudes. The skin friction based on viscous resistance in the wall environment is defined:

$$C_f = \frac{\tau_w}{\rho v w^2}$$

where

$$\tau_w = \left(\mu_B + \frac{P_y}{\sqrt{2\pi}}\right)\frac{\partial u}{\partial y}|_\eta = 0$$

$$(Re)^{\frac{1}{2}} C_f = \left(1 + \frac{1}{\beta}\right) f''(0)$$

The heat transport rate (Nusselt number) based on the heat transport between the liquid and the wall is

$$Nu = \frac{q_w}{K(T)(T_w - T_\infty)} = \theta'(0)$$

where

$$q_w = k\left(\frac{\partial T}{\partial y}\right)_{y=0} = \alpha(T_w - T_\infty)\theta'(0)$$

The mass transport rate originates from the Sherwood number, defined as

$$Sh = \frac{d_w}{D(T)(C_w - C_\infty)} = \phi'(0)$$

where

$$d_w = D(T)\left(\frac{\partial C}{\partial y}\right)_{y=0} = D(T)(C_w - C_\infty)\phi'(0)$$

2. NUMERICAL SOLUTION

The Chebyshev spectral collocation method was applied to acquire a mathematical solution for the present system of nonlinear differential equations. (19) – (21) with boundary conditions (22)-(23). In this method, the functions, $f(\eta) = \sum_{i=o}^{N} a_i T_i(\eta)$, $\theta(\xi) = \sum_{i=o}^{N} b_i T_i(\eta)$ $\phi(\eta) = \sum_{i=o}^{N} c_i T_i(\eta)$ and are approximated by the sum of the basic functions $T_n(\eta)$. The basis functions are chosen as the Chebyshev polynomials $T_n(\eta) = \cos\left(N \cos^{-1}\eta\right)$, $-1 \le \eta \le 1$, where a_n, b_n and c_n are unknown constants to be obtained. The domain of the flow model $[0, \infty]$ is therefore transformed into $[-1,\ 1]$ the definition of basis functions, with the help of $\eta = {2\xi}/{\xi_\infty} - 1$ where ξ_∞ denotes the edge of the boundary layer. Now, to obtain the non-zero residual, we substitute the values of $f(\eta), \theta(\eta), and\ \phi(\eta)$ into Eqs. (10) – (12), where the coefficient a_i b_i s and c_i were chosen in such a manner that the obtained residues were minimised throughout the domain. The present model employed the collocation point method with the collocation points expressed by Akaje and Olajuwon [20]:

$$\eta_i = \cos\left(\frac{i\pi}{Z}\right), \quad i = 0,1,2,3..Z \qquad (24)$$

This generates a system of $3i+3$ algebraic equations along with $3i+3$ unknown coefficients a_i, b_i, and c_i. Newton's iteration method was employed for $i = 30$. Further, this algorithm for the boundary value problem is developed in Mathematical software to produce the numerical results.

RESULT AND DISCUSSION

The transformed coupled differential equations (19)— (21) alongside the boundary conditions (22) and (23) have been numerically solved by utilizing a spectral-based method called the collocation method. The significance of pertinent flow parameters on temperature$(\theta(\eta))$, concentration $(\phi(\eta))$ and velocity $\left(1+\frac{1}{\beta}\right)f'$ is presented using graphs, while physical quantities of engineering interest are presented using tables. The effect of the nonlinear thermal Grashof number (α_1) is illustrated in Figure 2. The nonlinearity of the thermal Grashof number gives an upward elevation of the fluid velocity profile very close to the wall. Physically, from Figure 2. The increment diminishes far away from the plate. This shows that, as $\eta \longrightarrow \infty$, the significance of α_1 is negligible. Furthermore, the nonlinearity of the buoyant force provides a greater upward force exerted by the object displaced in the fluid. Figure 3 depicts the significance of the nonlinear mass Grashof number (α_2) on the velocity profile. An increase in α_2 is noticed to elevate the hydrodynamic boundary layer and the fluid velocity profile. Physically, pressure increases due to the concentration of mass in depth. The pressure applied at the bottom becomes much greater than the force experienced at the top.

Figure 4 illustrates the effect of the Casson parameter (β) on the velocity profile. A drastic increase in velocity is observed from Figure 4 as the value of β increases. Physically, $\xi_1 = \xi_2 = 0$ indicates constant viscosity and thermal conductivity. In this case, where $\xi_1 = \xi_2 = 3$, the fluid velocity increases close to the plate and diminishes gradually far from the plate. A higher Casson parameter produces a very high resistance to the flow of fluid, but as a result of varying the viscosity and thermal conductivity, an enhancement in fluid velocity is noticeable in Figure 4. Physically, variable viscosity introduces a temperature-dependent shear thinning effect as temperature rises near the wall, viscosity decreases exponentially, thereby reducing the effective yield stress of the Casson fluid. The reduction in viscosity lowers internal frictional resistance, which counterbalances the restrictive influence of the Casson parameter. Consequently, the apparent viscosity gradient near the surface dominates, promoting fluid acceleration and enhancing the velocity field. This observation agrees with Idowu and Falodun (2020), who reported that temperature-dependent viscosity can invert the conventional Casson parameter effect on flow dynamics. A significant impact of the chemical reaction parameter is illustrated in Figure 5. An increase in the chemical reaction parameter (Cr) is observed to decrease the velocity and concentration distributions. This is because the reaction rate dominates diffusion coefficients.

Figure 6 shows the impact of the Eckert number (Ec) on the velocity and temperature profiles. In the energy equation, the Eckert number is derived from the viscous dissipation term, which is a function of velocity. It is the relationship between kinetic energy and the enthalpy in the working fluid. A large EC leads to shearing forces in the fluid. A large Ec leads to a larger variable viscosity and thermal conductivity, which produces heat energy to raise the thermal boundary layer thickness.

Figure 7 depicts the effect of thermal relaxation term(γ) on the velocity and temperature profiles. An increase in γ is noticed to enhance the velocity and temperature profiles. The time employed for fluid particles to diffuse rises due to the variable viscosity and thermal conductivity. Figure 8 illustrates the significance of the modified Hartman factor (M_q) on the velocity profile. The penetrable Riga plate produces Lorentz forces, which give surface tension. Due to this tension, an enhancement in the velocity was observed. Figure 9 illustrates the impact of the Prandtl number on the velocity and temperature profiles. A higher value of Pr is observed to degenerate the velocity and temperature profiles. These show a decrease in the thermal boundary layer thickness, as shown

in Figure 9. Hence, the thermal diffusion rate decreases because of the increase in Prandtl number. Figure 10 shows the effects of thermal radiation parameter(R) on the velocity and temperature profiles. An increase in R is observed to increase the velocity and temperature distribution. This implies that an increase in R indicates an enhancement in the thermal condition of the fluid.

Figure 11 depicts the effect of Schmidt number (Sc) on the velocity and concentration profiles. The Schmidt number is the ratio of the kinematic viscosity to the mass diffusivity of the fluid. An increase in Sc reduces the concentration buoyancy effects, which lead to a decrease in velocity and temperature.

Figure 12 illustrates the impact of the thermophoresis parameter (τ)on the velocity and concentration profiles. Due to the variable viscosity and thermal conductivity, an increase in velocity and temperature is observed in Figure 12. Physically, an increase in τ results in thickness in the concentration boundary layer and thereby enhances the rate of mass transfer. Figure 13 shows the impact of variable viscosity on the velocity profile. A larger value of the variable viscosity parameter (ξ_1) is observed to elevate the fluid velocity. Varying the viscosity within the boundary layer enhances the hydrodynamic boundary layer. Figure 14 shows the effect of variable thermal conductivity on the fluid temperature. Raising the variable thermal conductivity enhances the velocity of the hydrodynamic boundary layer, temperature and thermal boundary layer thickness. In Figure 15, the velocity of fluid at the riga surface was found to increase due to an increase in the riga surface term. Table 2 shows the comparison of the present result with that of Falodun and Omowaye [17]. Figure 15 shows the significant effect of the Brownian motion parameter on the velocity and temperature profiles. An increase in Nb is observed to increase the velocity and temperature profiles. Physically, when the particles are in constant motion, all particles will not be able to settle down, and this leads to the colloidal solution stability. Hence, increasing the Brownian motion parameter enhances the velocity of the fluid particles (the random collision).

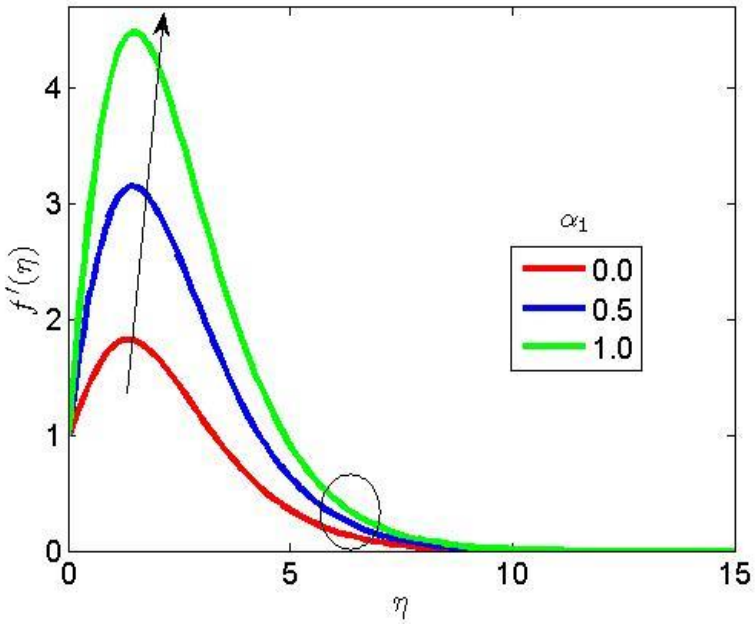

Figure 2: Effect of the nonlinear thermal Grashof number on the velocity profile

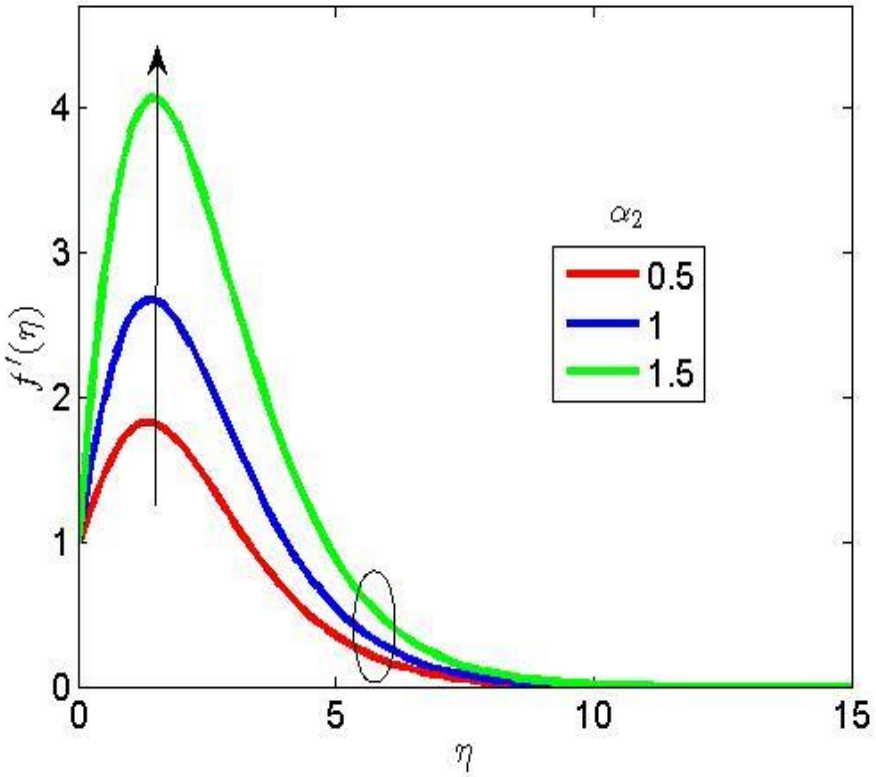

Figure 3: Effect of nonlinear mass Grashof number on the velocity profile

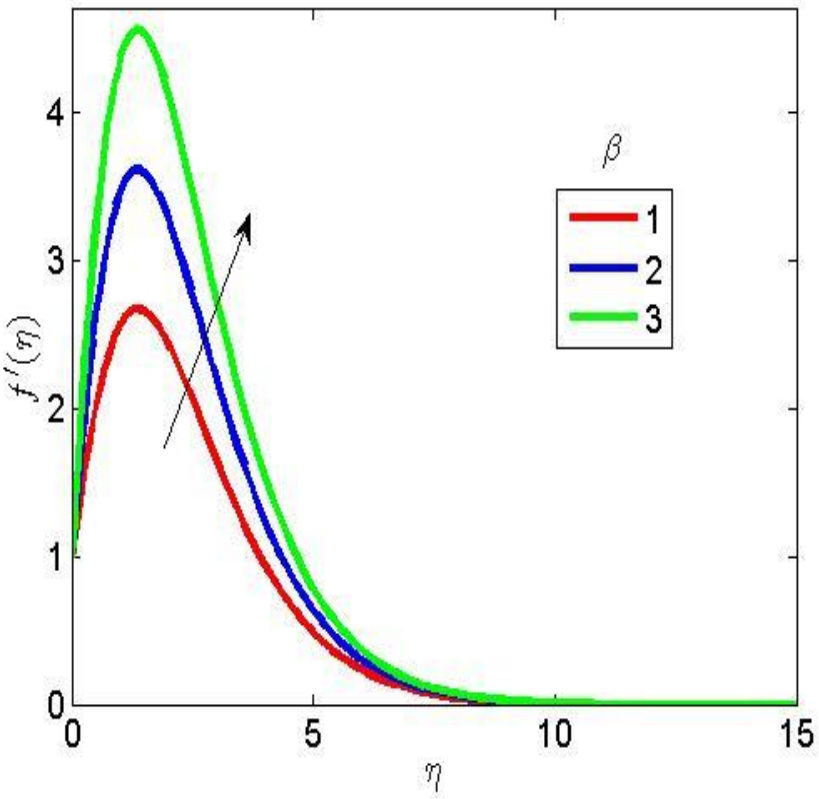

Figure 4: Effect of Casson parameter on the velocity profile

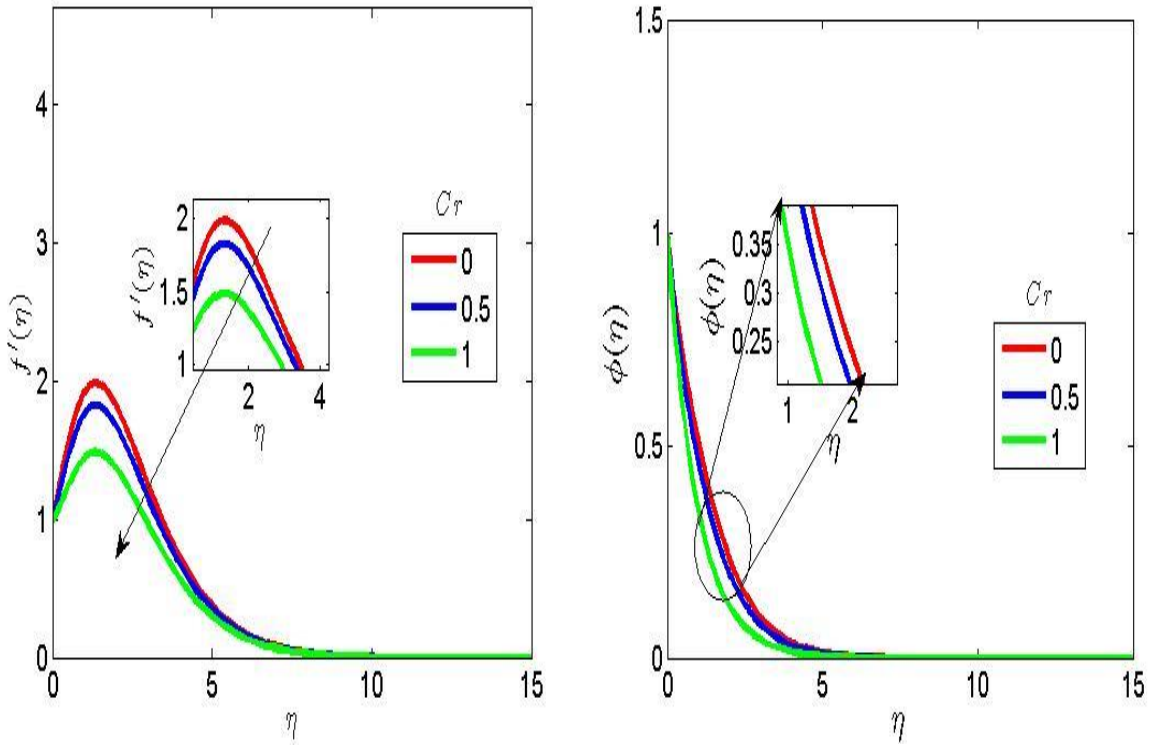

Figure 5: Effect of the chemical reaction parameter on the velocity and concentration profiles

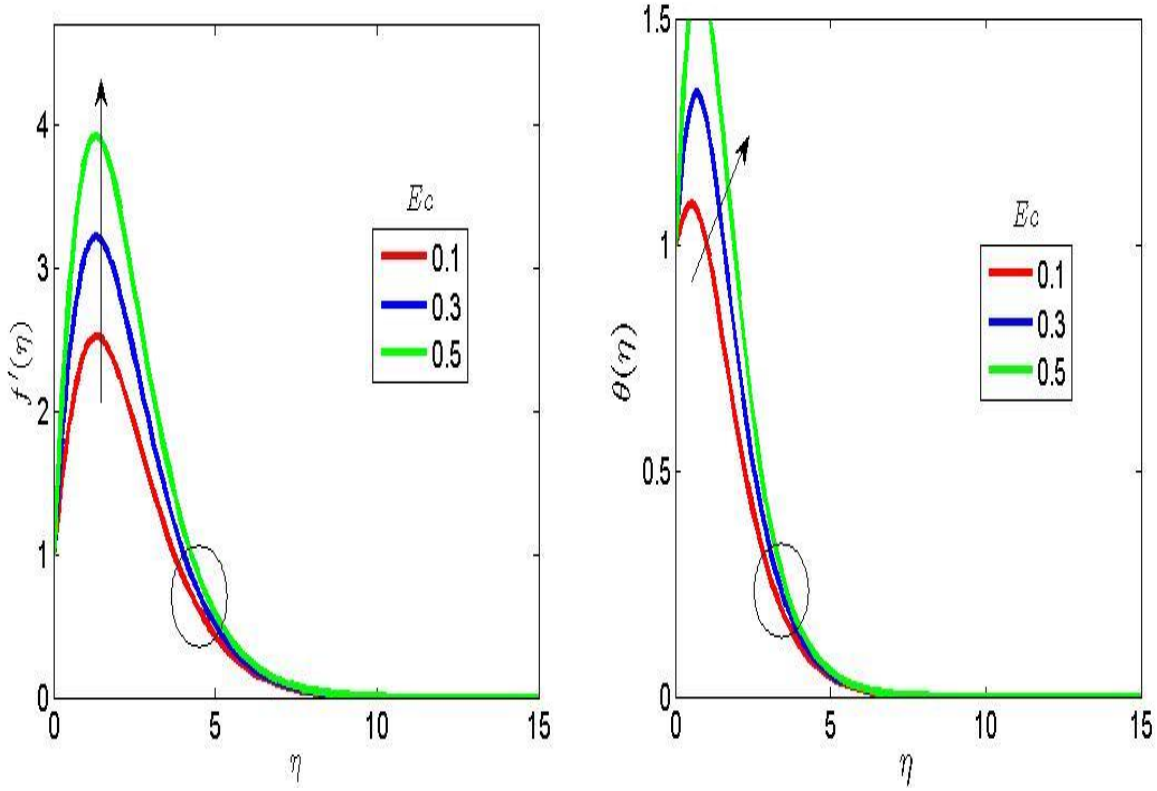

Figure 6: Effect of the Eckert number on the velocity and temperature profiles

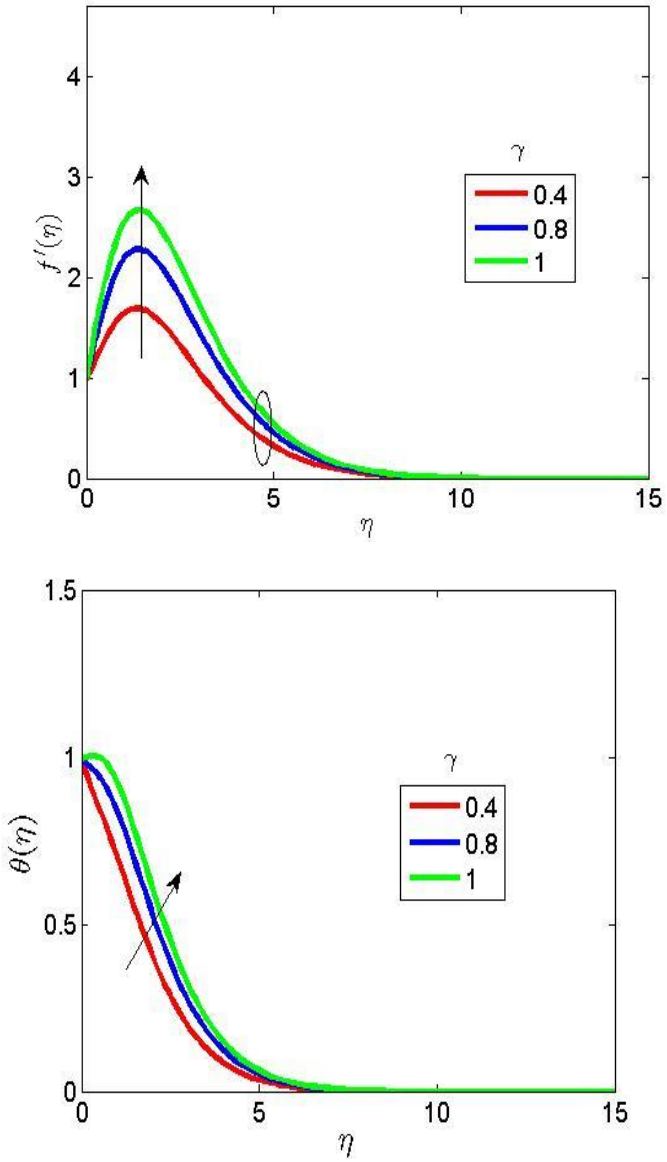

Figure 7: Effect of the thermal relaxation term on the velocity and temperature profiles

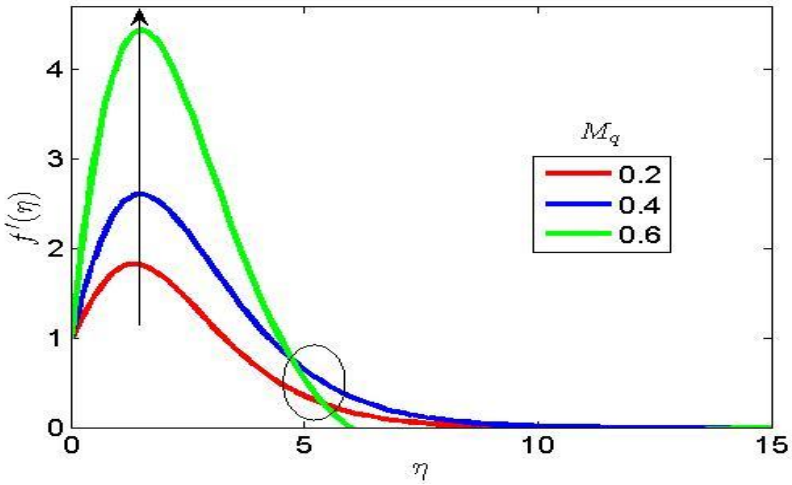

Figure 8: Effect of modified Hartman number on the velocity profile

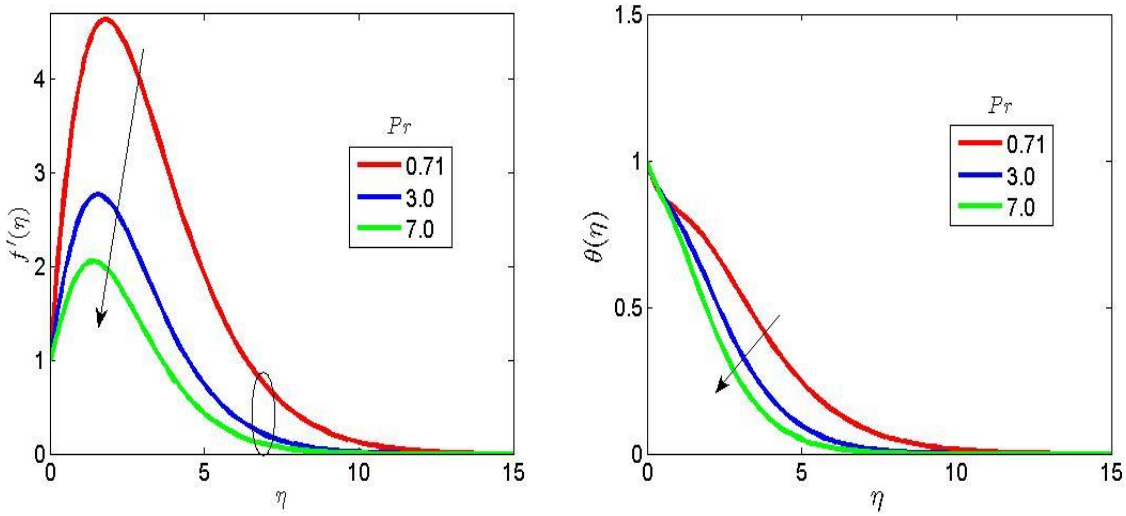

Figure 9: Effect of Prandtl number on the velocity and temperature profiles

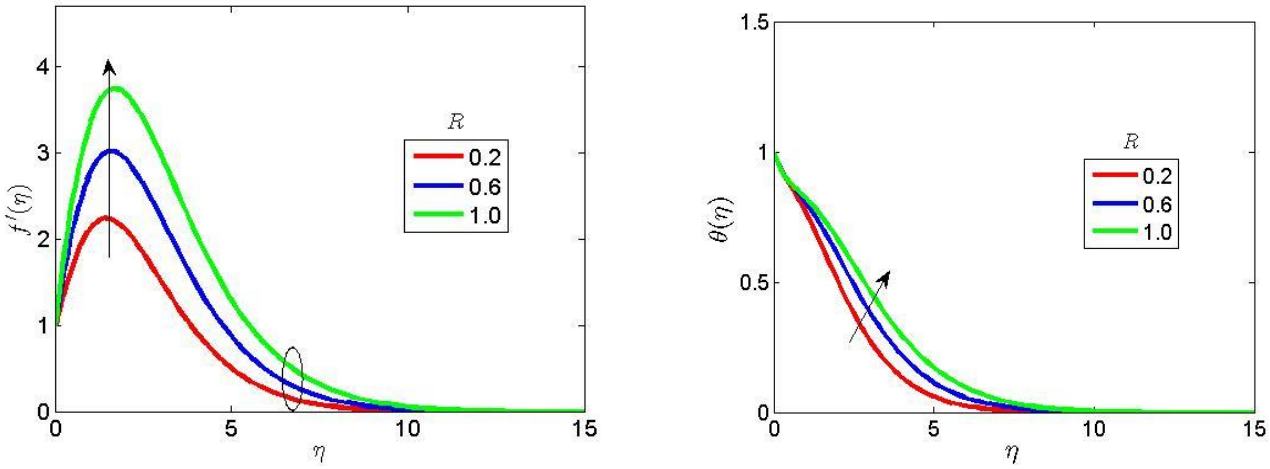

Figure 10: Effect of thermal radiation on the velocity and temperature profiles

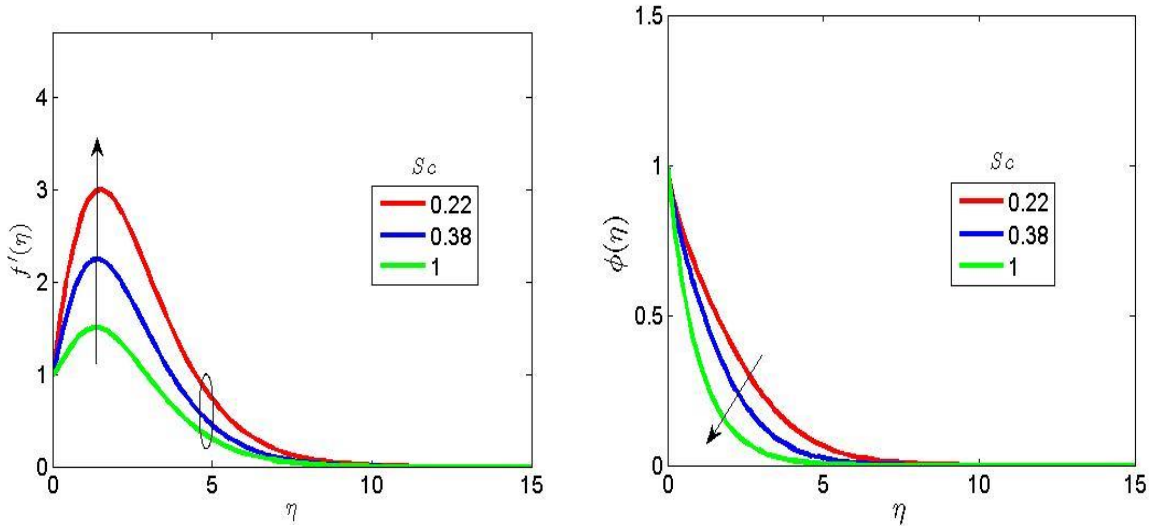

Figure 11: Effect of the Schmidt number on the velocity and concentration profiles

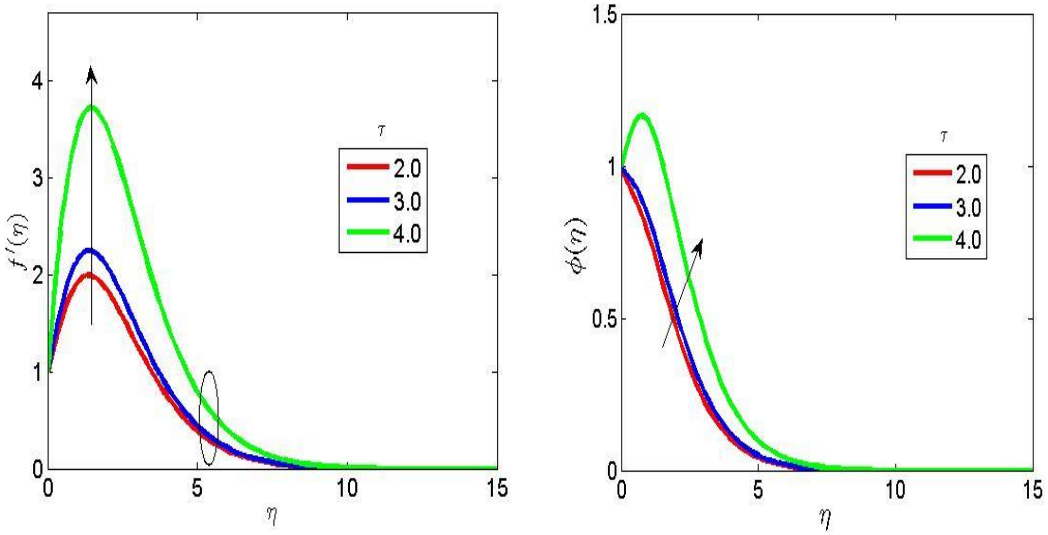

Figure 12: Effect of thermophoresis parameter on the velocity and concentration profiles

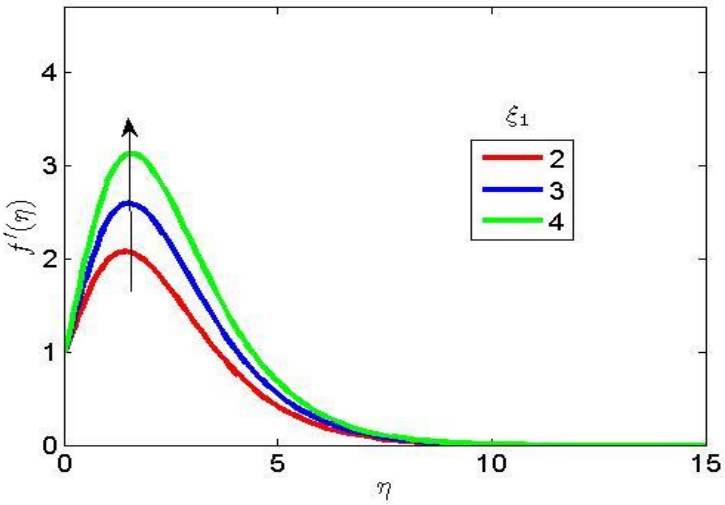

Figure 13: Effect of variable viscosity parameter on the velocity profile

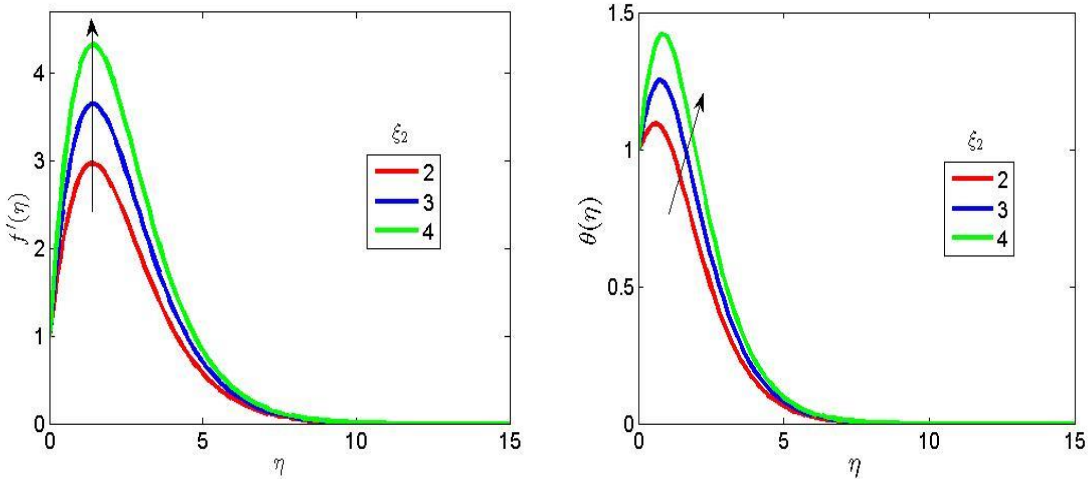

Figure 14: Effect of variable thermal conductivity on the velocity and temperature profiles

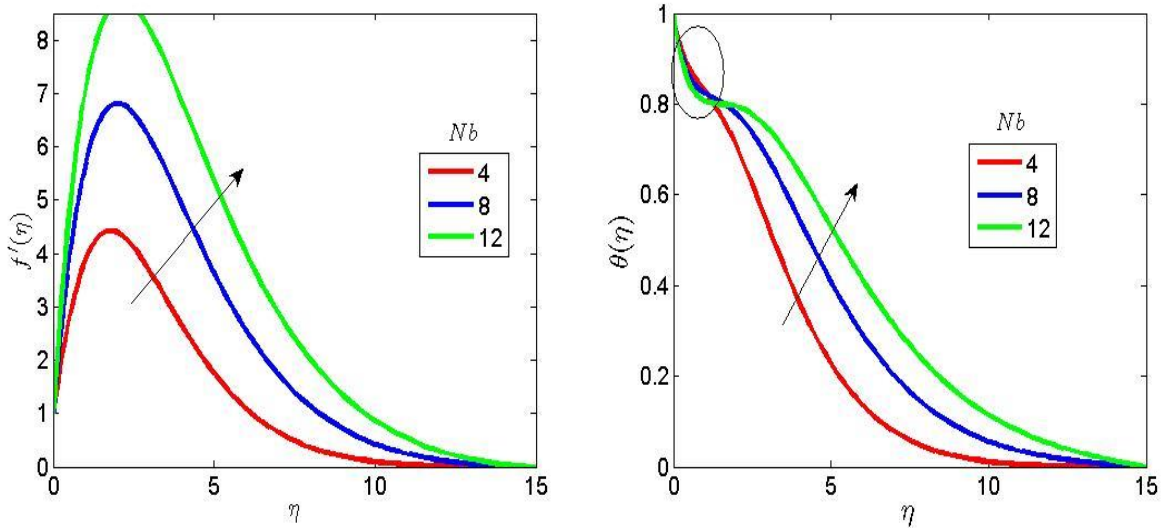

Figure 15: Effect of Brownian motion parameter on the velocity and temperature profiles

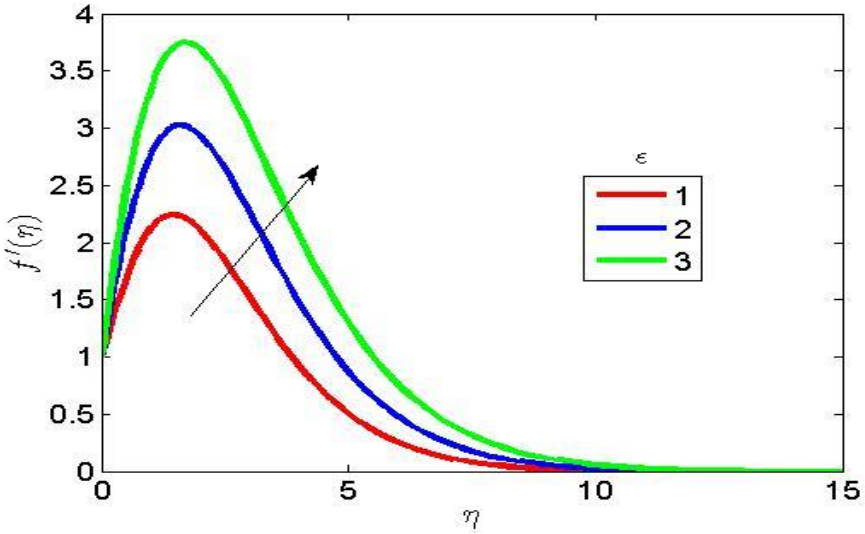

Figure 16: Effect of the riga surface term on the velocity profile

Table 1: Computational values of flow parameters on skin friction, Nusselt number and Sherwood number.

β	ξ_1	ξ_2	α_1	α_2	Pr	R	Ec	γ	Cr	Sc	τ	M_q	C_f	Nh	Sh
1.0													0.7555	0.3371	0.2074
2.0													2.3307	0.3371	0.2074
3.0													3.9058	0.3371	0.2074
	2.0												1.3434	0.9321	0.7999
	3.0												2.7060	0.9321	1.8569
	4.0												4.0687	0.9321	2.6379

		2.0											1.1989	0.2426	0.6105
		3.0											2.2937	0.5718	0.6105
		4.0											3.3885	0.9911	0.6105
			0.0										0.6621	0.4172	0.6001
			0.5										0.3746	0.4172	0.6001
			1.0										1.4113	0.4172	0.6001
				0.0									0.6621	0.4373	0.5691
				0.5									0.7126	0.4373	0.5691
				1.0									2.9503	0.4373	0.5691
					0.71								2.9483	0.3998	0.5110
					1.0								0.6115	0.3537	0.5110
					3.0								0.3378	0.3397	0.5110
						0.2							0.0845	0.3427	0.7569
						0.6							0.9431	0.3597	0.7569
						1.0							1.8569	0.3777	0.7569
							0.1						0.5565	0.2584	0.8010
							0.3						1.7755	0.8541	0.8010
							0.5						2.9945	1.4498	0.8010
								1.0					0.8710	0.3897	0.7977
								2.0					0.7126	0.1581	0.7977
								3.0					0.0864	0.0176	0.7977
									0.0				0.3897	0.7141	0.6951
									0.5				0.6621	0.7141	0.7977
									1.0				1.2266	0.7141	1.0361
										0.22			0.0223	0.4168	0.5993
										0.38			1.0173	0.4168	0.6760
										0.61			1.1911	0.4168	1.0274

											2.0		0.0300	0.1712	0.0569
											3.0		0.3863	0.2696	0.0569
											4.0		2.4042	0.3318	0.0569
												0.0	0.6621	0.4168	0.7600
												0.5	0.1846	0.4168	0.7600
												1.0	2.6853	0.4168	0.7600

Table 2: The comparison of the present result with the study of Falodun and Omowaye [17]when $\xi_1 = \xi_2 = \gamma = \beta = M_q = \alpha_1 = \alpha_2 = Do = So = He = Ln = \tau = Nb = Nt = 0$

M	Present study			Falodun and Omowaye [17]		
	$-f'(0)$	$-\theta'(0)$	$-\phi'(0)$	$-f'(0)$	$-\theta'(0)$	$-\phi'(0)$
0.0	1.21162128	0.59172595	2.80851597	1.21162126	0.59172595	2.80851598
0.5	1.35842065	0.58861362	2.81200612	1.35842063	0.58861361	2.81200613
1.0	1.49482307	0.58611502	2.81550164	1.49482305	0.58611501	2.81550165
2.0	1.74371571	0.58195571	2.82145443	1.74371569	0.58195570	2.82145444

CONCLUSION

This study has considered incompressible laminar Casson fluid flow along a chemically reacting Riga surface with Cattaneo-Christov heat flux. No-slip boundary conditions have been utilized alongside thermophoresis and first-order chemical reactions. The model was solved using the spectral collocation technique, and the following are the major findings:

(i) A decrease in the velocity and concentration profile is observed due to an increase in chemical reaction parameters. The modified Hartman number (M_q) is observed to enhance the profile and the entire hydrodynamic boundary layer.

(ii) An increase in the Prandtl number is observed to decrease the velocity and temperature profile.

(iii) The velocity and the concentration distributions are observed to decrease due to an increase in Schmidt number; and

(iv) An increase in the thermal radiation and Eckert number is observed to increase the velocity, temperature, and thermal condition of the fluid.

REFERENCES

[1] Raju C.S.K., Sandeep N., Saleem S. (2016). Effects of induced magnetic field and homogeneous–heterogeneous reactions on stagnation flow of a Casson fluid. *Engineering Science and Technology, an International Journal, 19, 875–887.*

[2] Mahanta G., Shaw S. (2015). 3D Casson fluid flow past a porous linearly stretching sheet with convective boundary condition. *Alexandria Engineering Journal, 54, 653–659.*

[3] Bhatti M.M., Abbas M.A., Rashidi M.M. (2017). Entropy generation for peristaltic blood flow with Casson model and consideration of magnetohydrodynamics effects. *Walailak Journal of Science and Technology, 14(6), 451–461.*

[4] Makanda G., Shaw S., Sibanda P. (2015). Diffusion of chemically reactive species in Casson fluid flow over an unsteady stretching surface in a porous medium in the presence of a magnetic field. *Mathematical Problems in Engineering, 2015:724596.*

[5] Rashidi M.M., Ali M., Rostami B., Rostami P., Xie G.-N. (2015). Heat and mass transfer for MHD viscoelastic fluid flow over a vertical stretching sheet, considering Soret and Dufour effects. *Mathematical Problems in Engineering, 2015:861065.*

[6] Idowu A.S., Falodun B.O. (2020). Variable thermal conductivity and viscosity effects on non-Newtonian fluid flow through a vertical porous plate under Soret–Dufour influence. *Mathematics and Computers in Simulation, 177, 358–384.*

[7] Falodun B.O., Onwubuoya C., Awoniran A.F.H. (2017). Magnetohydrodynamics (MHD) heat and mass transfer of Casson fluid flow past a semi-infinite vertical plate with thermophoresis effect: Spectral relaxation analysis. *Defect and Diffusion Forum, 389, 18–35.*

[8] Waqas H., Farooq U., Naseem R., Hussain S., Alghamdi M. (2021). Impact of MHD radiative flow of hybrid nanofluid over a rotating disk. *Case Studies in Thermal Engineering, 26, 101015.*

[9] Zhang X.H., Algehyne A.E., Alshehri G.M., Bilal M., Khan M.A., Muhammad T. (2021). Parametric study of hybrid nanofluid flow with heat transition characteristics over a fluctuating spinning disk. *PLoS ONE, 16(8):e0254457.*

[10] Ramzan M., Dawar A., Saeed A., Kumam P., Watthayu W., Kumam W. (2021). Heat transfer analysis of the mixed convective flow of a magnetohydrodynamic hybrid nanofluid past a stretching sheet with velocity and thermal slip conditions. *PLoS ONE, 16(12):e0260854.*

[11] Jamshed W., Nisar K.S., Ibrahim R.W., Mukhtar T., Vijayakumar V., Ahmad F. (2021). Computational framework of Cattaneo–Christov heat flux effects on engine-based Williamson hybrid nanofluids: A thermal case study. *Case Studies in Thermal Engineering, 26, 101179.*

[12] Kumar R., Sood S., Raju C.S.K., Shehzad S.A. (2019). Hydromagnetic unsteady slip stagnation flow of nanofluid with suspension of mixed bio-convection. *Propulsion and Power Research, 8(4), 362–372.*

[13] Ali M.E., Sandeep N. (2017). Cattaneo–Christov model for radiative heat transfer of magnetohydrodynamic Casson-ferrofluid: A numerical study. *Results in Physics, 7, 21–30.*

[14] Loganathan P., Deepa K. (2020). Computational exploration of Casson fluid flow over a Riga plate with variable chemical reaction and linear stratification. *Nonlinear Analysis: Modelling and Control, 25(3), 443–460.*

[15] Eswaramoorthi S., Alessa N., Sangeethavaanee M., Namgyel N. (2021). Numerical and analytical investigation for Darcy–Forchheimer flow of a Williamson fluid over a Riga plate with double stratification and Cattaneo–Christov dual flux. *Advances in Mathematical Physics, 2021, 1867824.*

[16] Rasool G., Zhang T. (2019). Characteristics of chemical reaction and convective boundary conditions in Powell–Eyring nanofluid flow along a radiative Riga plate. *Heliyon, 5:e01479.*

[17] Falodun B.O., Omowaye M. (2019). Double-diffusive MHD convective flow of heat and mass transfer over a stretching sheet embedded in a thermally-stratified porous medium, *World Journal of Engineering* (2019) 16 (6): 712–724.

[18] Akaje T.W., Olajuwon B.I. and Raji, M.T. (2023). Computational analysis of the heat and mass transfer in a casson nanofluid with a variable inclined magnetic field, *Sigma J Eng Nat Sci, Vol. 41, No. 3, pp. 512-523.*

[19] Akaje T.W., Olajuwon B.I. (2023). Dynamics of a swimming microorganism-saturated blood flow under the influence of an inclined magnetic field and heat source. *Computational Thermal Sciences: An International Journal, 15(3).*